

# Magnetic and electronic transitions in monolayer electride $\text{Gd}_2\text{C}$ induced by hydrogenation: A first-principles study

Duo Xu, Jian-Feng Zhang, Zhong-Yi Lu<sup>✉,\*</sup> and Kai Liu<sup>✉†</sup>

*Department of Physics and Beijing Key Laboratory of Opto-electronic Functional Materials & Micro-nano Devices, Renmin University of China, Beijing 100872, China*

 (Received 12 March 2022; revised 7 July 2022; accepted 8 July 2022; published 26 July 2022)

The recently synthesized two-dimensional electride  $\text{Gd}_2\text{C}$  was proposed to be a ferromagnetic metal that possesses multiple pairs of Weyl points and may display a large anomalous Hall conductivity [Liu *et al.*, *Phys. Rev. Lett.* **125**, 187203 (2020)]. In view of its layered structure, here we carry out first-principles studies on the magnetic and electronic properties of  $\text{Gd}_2\text{C}$  in the ultrathin monolayer limit. We find that monolayer  $\text{Gd}_2\text{C}$  remains ferromagnetic like the bulk form and the hydrogenation can effectively tune its magnetism and electronic structure. With one-sided full coverage of hydrogen atoms, monolayer  $\text{Gd}_2\text{C}$  becomes a half-metal with one spin channel around the Fermi level. For two-sided full hydrogenation, monolayer  $\text{Gd}_2\text{C}$  transforms to an antiferromagnetic insulator with a band gap of 0.8 eV. Our studies show that monolayer electride  $\text{Gd}_2\text{C}$  can perform multiple magnetic and electronic transitions with different levels of hydrogenation and may be also adopted to construct a planar heterojunction with selective area adsorption of hydrogen atoms, which has promising applications in future electronic and spintronic devices.

DOI: [10.1103/PhysRevB.106.045138](https://doi.org/10.1103/PhysRevB.106.045138)

## I. INTRODUCTION

The electride materials are deemed to possess excess electrons, so-called free electron gas, serving as anions [1,2]. These excess electrons locate on the lattice voids but do not bind to certain nuclei [1,2]. According to the dimensionality of the free electron gas in the electrides, they can be classified into zero-dimensional, one-dimensional, two-dimensional (2D), and three-dimensional types [3]. The formation of an interstitial free electron gas is distinguished from the conventional covalent, ionic, or metallic bonds and can bring many interesting properties such as the low work function [4,5], high electronic mobility [6], high electron concentration [7], high density of active sites [8], and thermionic electron emission at low temperature [9], to name a few. On the other hand, some electrides can also demonstrate rich quantum phenomena such as metal-semiconductor transition [10], superconductivity [11], magnetism [12], nontrivial topological properties [1,2], etc. Because of their particular quantum phases and potential applications in widespread fields [13,14], the electride materials deserve more experimental and theoretical explorations.

A recent study [15] reported the successful synthesis of a ferromagnetic 2D electride  $\text{Gd}_2\text{C}$ , which has a Curie temperature of  $\sim 350$  K. The ferromagnetism of  $\text{Gd}_2\text{C}$  mainly comes from Gd  $4f$  electrons and the measured local moment on Gd is about  $7.26 \mu_B$  [16]. In comparison, the electronic states around the Fermi level are mainly contributed by Gd  $5d$  electrons and the free electron gas [15], which are also

spin polarized. A previous theoretical study predicted that the ferromagnetic  $\text{Gd}_2\text{C}$  can host multiple pairs of Weyl points around the Fermi level and exhibit a giant anomalous Hall conductivity (AHC) [17], which may have potential applications in future spintronic devices. In addition, a recent computational study suggested that an external electric field could alter the number of anionic electrons at the surface of few-layer  $\text{Gd}_2\text{C}$  [18]. With the reduced dimensionality, whether the physical properties of  $\text{Gd}_2\text{C}$  can be retained in the ultrathin limit and can be tuned via surface modification still needs investigation.

In this work, by using first-principles calculations, we have studied the magnetic and electronic properties of the electride material  $\text{Gd}_2\text{C}$  in its monolayer limit. Our calculations show that monolayer  $\text{Gd}_2\text{C}$  is still a ferromagnetic metal, resembling its bulk form. We have also investigated the influence of hydrogenation on monolayer  $\text{Gd}_2\text{C}$  to examine the possible magnetic transitions like hydrogenated graphene [19,20], hydrogenated monolayer  $\text{Ca}_2\text{N}$  [21], and chlorine-intercalated bulk  $\text{Gd}_2\text{C}$  [15]. We find that the one-sided full hydrogenation can completely suppress one spin channel around the Fermi level and drives  $\text{Gd}_2\text{C}$  to a ferromagnetic half-metal, while the two-sided full hydrogenation can transform  $\text{Gd}_2\text{C}$  to an antiferromagnetic insulator. The monolayer electride  $\text{Gd}_2\text{C}$  can thus perform multiple magnetic and electronic transitions at different levels of hydrogenation.

## II. METHOD

To investigate the electronic and magnetic properties of monolayer  $\text{Gd}_2\text{C}$  with hydrogenation, we carried out the density functional theory [22,23] calculations by using the Vienna Ab initio Simulation Package (VASP)[24,25]. Both

\*zlu@ruc.edu.cn

†kliu@ruc.edu.cn

the in-plane lattice constants and the internal atomic positions of the pristine and hydrogenated  $\text{Gd}_2\text{C}$  monolayers were fully relaxed until the forces on all atoms were smaller than  $0.01 \text{ eV/\AA}$ . The generalized gradient approximation (GGA) of the Perdew-Burke-Ernzerhof [26] type was adopted for the exchange-correlation functional. A kinetic energy cutoff of  $520 \text{ eV}$  was used for the plane-wave basis. A  $\mathbf{k}$ -point mesh of  $16 \times 16 \times 1$  was adopted for the Brillouin zone (BZ) sampling in the structural optimization calculations, and a fine grid of  $60 \times 60 \times 1$  was used in the self-consistent calculations. The Gaussian smearing method with a width of  $0.02 \text{ eV}$  was used for the Fermi surface broadening. To describe the strong correlation effect among Gd  $4f$  electrons, the GGA +  $U$  formalism [27] was adopted with an effective Hubbard  $U$  of  $6.0 \text{ eV}$ , the same as a previous theoretical study [17]. In phonon calculations, the real-space force constants were calculated within the density functional perturbation theory [28] as implemented in VASP [24,25] and the phonon dispersion was then calculated with PHONOPY [29]. The AHC of monolayer  $\text{Gd}_2\text{C}$  was studied within the Berry curvature scheme [30], which was implemented in the WANNI90 [31] and WANNIERTOOLS [32] packages:  $\sigma_{xy}^{2D} = -\frac{e^2}{h} \int_{\text{BZ}} \frac{dk_x dk_y}{(2\pi)^2} \Omega_{xy}(k)$ . Here  $\Omega_{xy}(k) = \sum_n f_n(k) \Omega_{n,xy}(k)$  is the total Berry curvature [30], where  $f_n(k)$  is the occupation factor and  $n$  is the index of energy band. The spin-orbit coupling (SOC) effect was included in the AHC and magnetic anisotropy energy (MAE) calculations, while its influence on the band structures was also examined (see Supplemental Material (SM) [33]).

### III. RESULTS

The calculated cleavage energy of  $\text{Gd}_2\text{C}$  is  $1.21 \text{ J/m}^2$ , which is slightly larger than that of  $\text{Ca}_2\text{N}$  ( $1.09 \text{ J/m}^2$ ) [34]. The comparable cleavage energies between these two electrides indicate that  $\text{Gd}_2\text{C}$  can be also reduced to the monolayer thickness via the liquid exfoliation method as  $\text{Ca}_2\text{N}$  [35]. According to the calculated phonon dispersion [Fig. 4(a) in the Appendix], the pristine  $\text{Gd}_2\text{C}$  monolayer has no imaginary frequency through the entire BZ, indicating its dynamical stability. We also performed the molecular dynamics (MD) simulations at  $300 \text{ K}$  and found that the structure of the  $\text{Gd}_2\text{C}$  monolayer was still compact (Fig. S2 in the SM [33]), suggesting that it is thermodynamically stable at room temperature. Since the Gd atom contains seven  $4f$  electrons, we studied several typical magnetic configurations of the  $\text{Gd}_2\text{C}$  monolayer (Fig. 5 in the Appendix), whose relative energies are listed in Table I. As can be seen, the ferromagnetic (FM) state is energetically most favorable for the pristine  $\text{Gd}_2\text{C}$  monolayer, being the same as its bulk crystal [17]. The total magnetic moment of the unit cell is  $15.94 \mu_B$ , mainly distributing on the Gd atoms. Moreover, the calculated energy differences between the FM and nonmagnetic states for monolayer and bulk  $\text{Gd}_2\text{C}$  are  $-19.08$  and  $-21.94 \text{ eV}$  per formula unit (f.u.), respectively. These results suggest that  $\text{Gd}_2\text{C}$  can retain stable and ferromagnetic in the monolayer limit [18].

Figure 1(a) shows the band structure of the pristine  $\text{Gd}_2\text{C}$  monolayer in the FM ground state, where both the spin-up (red lines) and spin-down (blue lines) channels cross the Fermi level, indicating its metallic characters. The inclusion

TABLE I. The relative energies (in units of  $\text{meV/f.u.}$ ) of typical magnetic configurations (Fig. 5 in the Appendix) with respect to their own FM states for different  $\text{Gd}_2\text{C}$  monolayers:  $\Delta E = E - E(\text{FM})$ . Here FM and AFM are abbreviations of ferromagnetic and antiferromagnetic, respectively. FM-FM means all Gd atoms are in ferromagnetic intralayer and interlayer couplings. Stripe and Zigzag stand for the stripe AFM and zigzag AFM intralayer couplings in the same Gd layers. The abbreviations ‘‘Semihydro.’’ and ‘‘Full hydro.’’ represent the semihydrogenation with one-sided H coverage and the full hydrogenation with two-sided H coverage, respectively.

$\Delta E$	Pristine	Semihydro.	Full hydro.
FM-FM	0.0	0.0	0.0
FM-AFM	164.5	81.1	-28.2
Stripe-FM	194.5	97.2	-28.2
Stripe-AFM	169.8	101.7	-16.5
Zigzag-FM	155.8	83.3	-25.8
Zigzag-AFM	158.5	94.3	-23.1

of the SOC only induces slight band splitting around the Fermi level (Fig. S1(a) in the SM [33]). From the partial density of states [Fig. 1(b)], both the Gd  $5d$  orbitals and the electron gas floating on the surface [Fig. 1(d)] have large contributions around the Fermi level. Interestingly, from the top view of the electron localization function (ELF) distribution in Fig. 1(d), the electron gas forms an approximate hexagonal pattern, while the crystal structure is still in  $C_3$  symmetry.

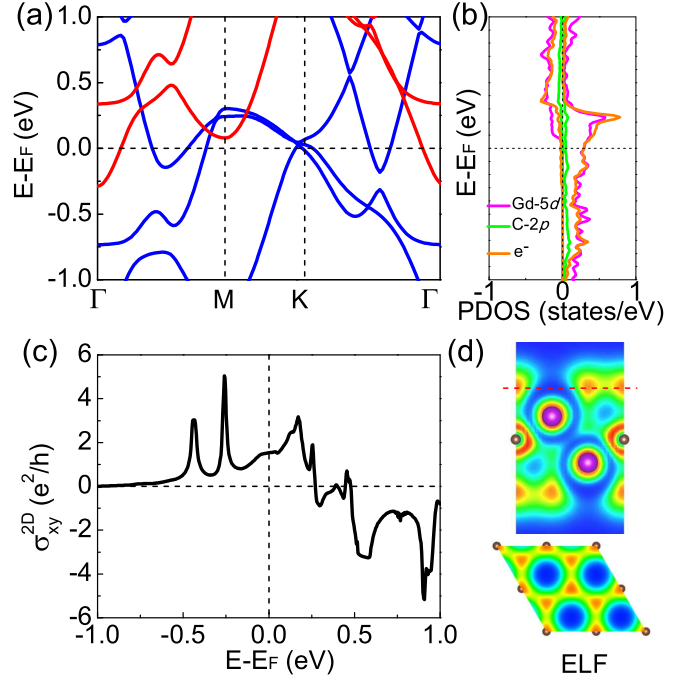


FIG. 1. (a) Electronic band structure of pristine  $\text{Gd}_2\text{C}$  monolayer. The red and blue lines represent the spin-up and spin-down channels, respectively. (b) Partial density of states (PDOS) of pristine  $\text{Gd}_2\text{C}$  monolayer. The pink, green, and orange lines label the states from Gd  $5d$ , C  $2p$ , and anionic electrons, respectively. (c) Calculated 2D anomalous Hall conductivity. (d) Electron localization function (ELF) distributions in the (110) and (001) planes. The latter is at a position above the surface labeled by the red dashed line.

This hexagonal pattern contains two lattice sites: one is on top of the C atom, the other is on top of the lower Gd atom. In comparison, the free electron gas in bulk  $\text{Gd}_2\text{C}$  condenses in the interlayer region and forms a triangular pattern in the ELF map [15]. As bulk  $\text{Gd}_2\text{C}$  was predicted to own a large intrinsic AHC with  $\sigma_{xy} = 399 \Omega^{-1} \text{cm}^{-1}$  at  $E_F$  [15], we also investigated the intrinsic 2D AHC  $\sigma_{xy}^{2D}$  of the pristine  $\text{Gd}_2\text{C}$  monolayer. From Fig. 1(c), the calculated  $\sigma_{xy}^{2D}$  at the Fermi level is about  $1.8 e^2/h$  ( $=0.698 \times 10^{-4} \Omega^{-1}$ ), which is larger than the ones of some traditional 2D ferromagnetic materials such as  $\text{Mn}_3\text{P}$  [37].

In order to regulate the magnetic and electronic properties, we have applied the lattice strain on the pristine  $\text{Gd}_2\text{C}$  monolayer. It turns out that when a 5% biaxial tensile strain is applied, the total magnetic moment of the unit cell increases slightly to  $16.02 \mu_B$  without introducing remarkable changes in the electronic band structure. This suggests that the magnetism of the pristine  $\text{Gd}_2\text{C}$  monolayer is not so sensitive to the lattice strain. Next, we try to adjust the physical properties of monolayer  $\text{Gd}_2\text{C}$  by other means.

It is well known that hydrogenation is a common way to tune the electronic and magnetic properties of layered materials. For example, the hydrogenation can drive the  $\text{MoO}_3$  nanoribbon from a semiconductor to a metal [38], induce the structural and magnetic transitions in  $\text{Ca}_2\text{N}$  monolayer [21], transform arsenene into a Dirac material [39], and induce high-temperature superconducting phases in iron-based superconductors [40]. In our study, because there is free electron gas located on both surfaces of the  $\text{Gd}_2\text{C}$  monolayer, hydrogenation will be an effective method to modulate the properties.

We first investigated the full coverage of hydrogen atoms on one side of the  $\text{Gd}_2\text{C}$  monolayer, namely, the semihydrogenation case. Multiple adsorption sites of H atoms were examined and the optimal site is on top of the lower Gd atom [Fig. 2(d)]. The adsorption energy at this site is  $124.9 \text{ meV/H}$  larger than at the other site (on top of C) of the approximate hexagonal lattice in Fig. 1(d). The dynamical stability of the semihydrogenated  $\text{Gd}_2\text{C}$  monolayer is also confirmed by the phonon calculation, in which no imaginary frequency is found in the whole BZ [Fig. 4(b) in the Appendix]. Meanwhile, the structure of the semihydrogenated  $\text{Gd}_2\text{C}$  monolayer is still compact in the MD simulations at 300 K (Fig. S2 in the SM [33]), suggesting its thermodynamical stability at room temperature. From the relative energies in Table I, we find that the optimal magnetic configuration of the semihydrogenated  $\text{Gd}_2\text{C}$  monolayer is still the FM state. The calculated band structure of the FM state is exhibited in Fig. 2(a). Notably, only one spin channel (blue lines) crosses the Fermi level, forming a ferromagnetic half-metal. Like the pristine case, the inclusion of SOC also causes slight band splitting around the Fermi level for the semihydrogenated  $\text{Gd}_2\text{C}$  monolayer (Fig. S1(b) in the SM [33]). By analyzing the projected DOS [Fig. 2(b)], we find that the two Gd atoms are not equivalent any more due to the asymmetrical adsorption of H atoms on one side. The calculated ELF distribution in Fig. 2(d) indicates that the free electron gas on one side of the  $\text{Gd}_2\text{C}$  monolayer transfers to the adsorbed H atoms and the electron gas on the other surface

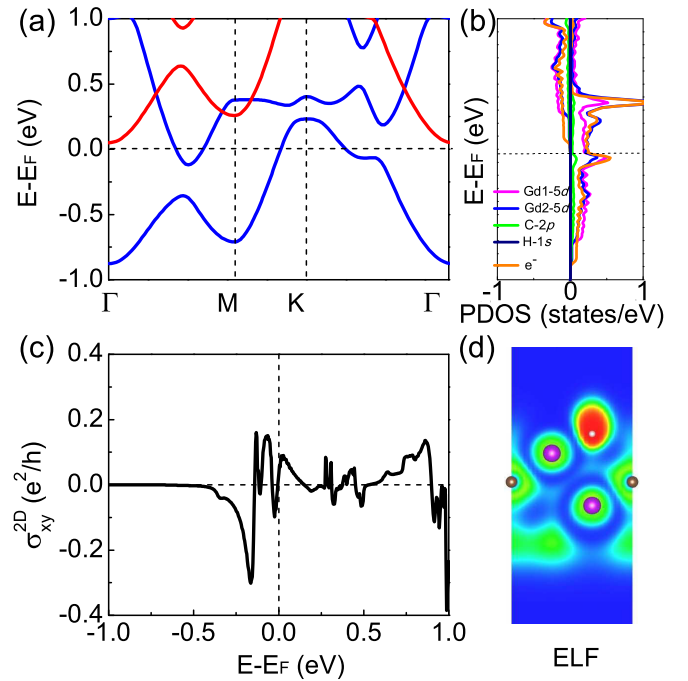


FIG. 2. (a) Electronic band structure of the semihydrogenated  $\text{Gd}_2\text{C}$  monolayer. The red and blue lines represent the spin-up and spin-down channels, respectively. (b) PDOS of the semihydrogenated  $\text{Gd}_2\text{C}$  monolayer. The pink, blue, green, and orange lines represent the states from the  $5d$  orbitals of upper and lower Gd atoms, C  $2p$  orbitals, and anionic electrons, respectively. (c) Calculated 2D AHC. (d) The ELF distribution in the (110) plane vertical to the  $\text{Gd}_2\text{C}$  monolayer.

is retained. The remaining free electron gas floating on the surface has a large contribution around  $E_F$  and shows strong spin polarization [Fig. 2(b)], similar to the pristine case [Fig. 1(b)]. In order to explore the electronic transport properties, we also calculated the intrinsic AHC  $\sigma_{xy}^{2D}$  as shown in Fig. 2(c). Compared with the pristine case [Fig. 1(c)], the AHC in the semihydrogenated  $\text{Gd}_2\text{C}$  monolayer decreases obviously. This variation may originate from the reduced number of Weyl points in Fig. 2(a), which weakens the magnitudes of Berry curvature  $\Omega_{xy}(k)$  and AHC.

When both sides of monolayer  $\text{Gd}_2\text{C}$  are covered with hydrogen atoms, the system becomes fully hydrogenated. According to the calculated phonon dispersion [Fig. 4(c) in the Appendix] and the structure snapshot in the MD simulation (Fig. S2 in the SM [33]), it is both dynamically and thermodynamically stable. By comparing the total energies of different magnetic configurations (Table I), we find that the magnetic ground state of the fully hydrogenated  $\text{Gd}_2\text{C}$  monolayer is either of the intralayer ferromagnetic coupling and the interlayer antiferromagnetic coupling [Fig. 5(b)] or of the intralayer stripe AFM coupling and the interlayer FM coupling [Fig. 5(c)]. The energy degeneracy of these two states originates from the equal number of AFM superexchange interactions between the Gd atoms in the upper and lower Gd layers via the bridging C atoms, namely, one C atom forming three AFM Gd (upper)-C-Gd (lower) bonds with six nearest-neighbor Gd atoms around it. The magnetism all comes from

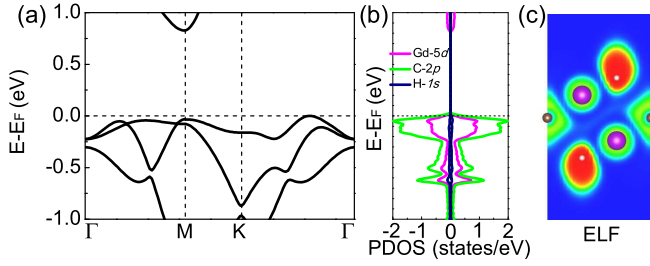


FIG. 3. (a) Electronic band structure and (b) PDOS of the fully hydrogenated  $\text{Gd}_2\text{C}$  monolayer in the FM-AFM state. The pink and green colors label the states from Gd  $5d$  and C  $2p$  orbitals. The signs represent different spin channels. (c) The ELF distribution in the (110) plane vertical to the  $\text{Gd}_2\text{C}$  monolayer.

the inner Gd  $4f$  shell with a  $7.09 \mu_B$  local moment, resulting in a zero net magnetic moment for the whole cell. From the band structures of the AFM ground state shown in Figs. 3(a) and 6(a), the fully hydrogenated  $\text{Gd}_2\text{C}$  monolayer is an insulator with a band gap of  $\sim 0.8$  eV, in sharp contrast to the pristine and semihydrogenated cases. This is because all the free electron gases on the surfaces of the  $\text{Gd}_2\text{C}$  monolayer are now localized around the adsorbed H atoms, as indicated by the ELF distribution in Figs. 3(c) and 6(c). According to the PDOS [Figs. 3(b) and 6(b)], C  $2p$  orbitals dominate the valence-band maximum, while Gd  $5d$  orbitals determine the conduction-band minimum. Besides, we also calculated the bands with the SOC. The original doubly degenerate bands are split with the inclusion of SOC; however, the system still remains insulating (Figs. S1(c) and S1(d) in the SM [33]). The above results indicate that the  $\text{Gd}_2\text{C}$  monolayer transforms into an antiferromagnetic insulator under the two-sided full hydrogenation.

We further studied the magnetic anisotropy of the  $\text{Gd}_2\text{C}$  monolayer without and with the hydrogenation. In the pristine  $\text{Gd}_2\text{C}$  monolayer, the easy magnetization axis is along the out-of-plane direction, similar to monolayer  $\text{CrI}_3$  [36]. With the destruction of central-inversion symmetry by the coverage of H atoms on one side, the easy magnetization axis of the semihydrogenated  $\text{Gd}_2\text{C}$  monolayer turns to in-plane as a result of the Rashba-type spin-orbit coupling [41]. The values of MAE are 0.663 and 0.236 meV/Gd in the pristine  $\text{Gd}_2\text{C}$  monolayer and the semihydrogenated  $\text{Gd}_2\text{C}$  monolayer, respectively. After H atoms cover on both sides, the magnetic anisotropy energy of the system becomes negligible, which may originate from the reduced interaction between localized Gd  $4f$  electrons in the insulating state for fully hydrogenated  $\text{Gd}_2\text{C}$ .

Finally, we considered the partial coverages of H atoms on the  $\text{Gd}_2\text{C}$  monolayer in addition to the above full coverages. Due to the inexhaustible possibilities and the computational cost, we only chose some representative examples to illustrate the effect of partial H coverage on the magnetic and electronic properties. Two partial ( $\frac{1}{4}$  and  $\frac{1}{9}$ ) coverages and two disordered coverages for the one-sided and two-sided hydrogenations were considered (see Figs. S3 and S4 in the SM [33]). From the calculated energies of these systems in different spin configurations (Tables S1 and S2 and Fig. S5 in the SM [33]), we find that they all possess the ferromagnetic ground states. Compared with the AFM ground state of the two-sided full H coverage, the FM ground state here suggests that the remaining free electron gas on the surface due to the incomplete H coverage is crucial to induce the ferromagnetic coupling between the Gd spins. According to the calculated DOSs of these ferromagnetic ground states (Figs. S6 and S7 in the SM [33]), they all show metallic characteristics. These results indicate that for the partial or disordered hydrogen coverages, no matter whether the  $\text{Gd}_2\text{C}$  monolayer is with the one-sided or the two-sided hydrogenation, they are all ferromagnetic metals.

#### IV. DISCUSSION AND SUMMARY

The monolayer electride  $\text{Gd}_2\text{C}$  and its hydrogenated forms have many advantages. First, the pristine  $\text{Gd}_2\text{C}$  monolayer has a stable FM state and may display a large AHC. Second, the semihydrogenated  $\text{Gd}_2\text{C}$  monolayer is an FM half-metal, which may be used as a spin filter to generate a 100% pure spin current. Third, the fully hydrogenated  $\text{Gd}_2\text{C}$  monolayer is an AFM insulator (I) that can realize the high switch ratio. Last but not least, with a selective area adsorption of hydrogen atoms, the  $\text{Gd}_2\text{C}$  monolayer can be processed to planar heterojunctions with the FM/I/FM modules. The diverse functionalities of the hydrogenated  $\text{Gd}_2\text{C}$  monolayer may thus have promising applications in future electronic and spintronic devices.

In summary, we have performed the first-principles electronic structure calculations on the ferromagnetic electride material  $\text{Gd}_2\text{C}$  in the monolayer limit. Our calculations indicate that the pristine  $\text{Gd}_2\text{C}$  monolayer is still a ferromagnetic metal, the same as its bulk form. Interestingly, we find that the coverage of hydrogen atoms on one side can suppress one of the spin channels and drive the  $\text{Gd}_2\text{C}$  monolayer into a ferromagnetic half-metal. After the full hydrogenation with two-sided coverage of H atoms, the  $\text{Gd}_2\text{C}$  monolayer will

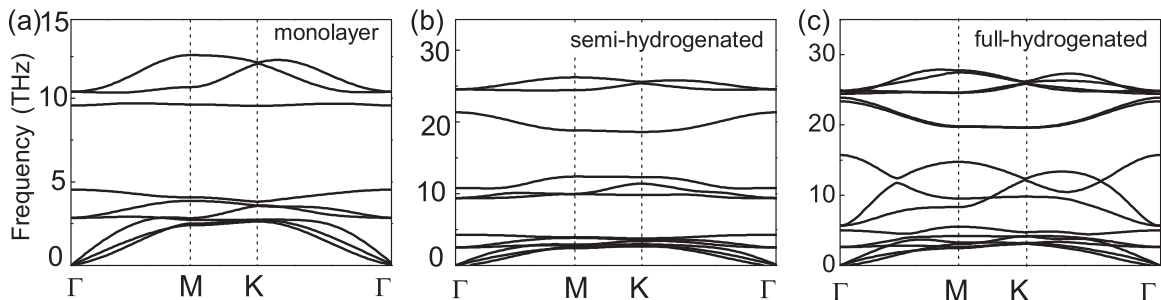


FIG. 4. Calculated phonon dispersions of the (a) pristine, (b) semihydrogenated, and (c) fully hydrogenated  $\text{Gd}_2\text{C}$  monolayers.

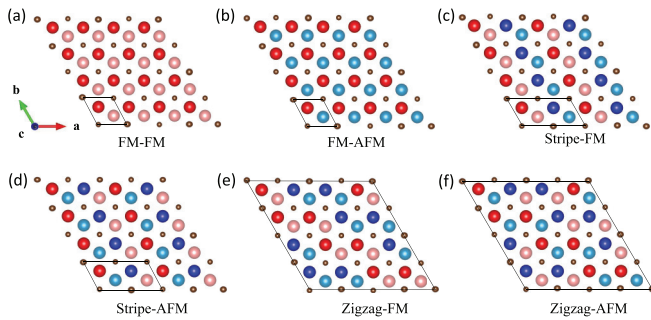


FIG. 5. Typical magnetic configurations for the Gd triangular lattices in monolayer  $\text{Gd}_2\text{C}$ . The red (blue) and light-red (light-blue) balls represent the spin-up (spin-down) Gd atoms in the upper and lower Gd layers, respectively. The brown balls represent the C atoms in the middle layer. The solid parallelograms label the unit cells of these magnetic structures.

further transfer to an antiferromagnetic insulator. We also calculate the anomalous Hall conductivity for the pristine and semihydrogenated  $\text{Gd}_2\text{C}$  monolayers, where the former shows a large value of  $1.8 e^2/h$ , superior to traditional 2D ferromagnetic materials. Further calculations indicate that the pristine  $\text{Gd}_2\text{C}$  monolayer has an out-of-plane easy axis of magnetization and the semihydrogenated one has an in-plane easy axis. In contrast, the magnetic anisotropy is insignificant for the full hydrogenation case. The versatile magnetic and electronic properties induced by the hydrogenation of the monolayer electride  $\text{Gd}_2\text{C}$  may thus be applied to future miniaturized electronic and spintronic devices.

#### ACKNOWLEDGMENTS

This work was supported by the National Key R&D Program of China (Grants No. 2017YFA0302903 and

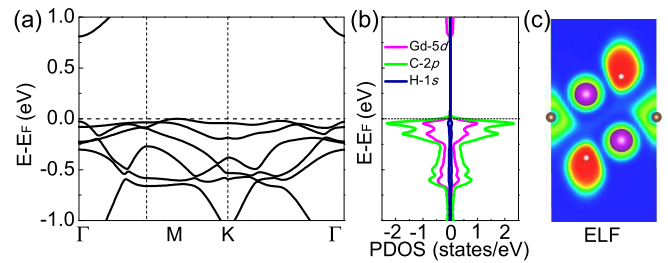


FIG. 6. (a) Electronic band structure and (b) PDOS of the fully hydrogenated  $\text{Gd}_2\text{C}$  monolayer in the stripe-FM state (Table I). The pink and green colors label the states from Gd  $5d$  and C  $2p$  orbitals. The signs represent different spin channels. (c) The ELF distribution in the (110) plane vertical to the  $\text{Gd}_2\text{C}$  monolayer.

No. 2019YFA0308603), the National Natural Science Foundation of China (Grants No. 11774424, No. 11934020, and No. 12174443), the Beijing Natural Science Foundation (Grant No. Z200005), the Fundamental Research Funds for the Central Universities, and the Research Funds of Renmin University of China (Grant No. 19XNLG13). Computational resources were provided by the Physical Laboratory of High Performance Computing at Renmin University of China.

#### APPENDIX

Figure 4 shows the calculated phonon dispersions for the pristine, semihydrogenated, and fully hydrogenated  $\text{Gd}_2\text{C}$  monolayers, none of which has the imaginary phonon mode.

Figure 5 displays the typical magnetic configurations for the Gd triangular lattices in the  $\text{Gd}_2\text{C}$  monolayer, whose relative energies are listed in Table I.

Figure 6 shows the electronic structure of the fully hydrogenated  $\text{Gd}_2\text{C}$  monolayer in the stripe-FM state (Table I), which is also an AFM insulator as the FM-AFM state (Fig. 3).

- [1] H. Hosono and M. Kitano, *Chem. Rev.* **121**, 3121 (2021).
- [2] X.-H. Zhang and G.-C. Yang, *J. Phys. Chem. Lett.* **11**, 3841 (2020).
- [3] Y.-W. Zhang, H. Wang, Y.-C. Wang, L.-J. Zhang, and Y.-M. Ma, *Phys. Rev. X* **7**, 011017 (2017).
- [4] S. Matsuishi, S. W. Kim, T. Kamiya, M. Hirano, and H. Hosono, *J. Phys. Chem. C* **112**, 4753 (2008).
- [5] S. Matsuishi, Y. Toda, M. Miyakawa, K. Hayashi, T. Kamiya, M. Hirano, I. Tanaka, and H. Hosono, *Science* **301**, 626 (2003).
- [6] D. I. Badrtdinov and S. A. Nikolaev, *J. Mater. Chem. C* **8**, 7858 (2020).
- [7] F. Li, X. Zhang, H.-L. Liu, J.-P. Zhao, Y.-X. Xiao, Q. Feng, and J.-X. Zhang, *J. Am. Ceram. Soc.* **102**, 884 (2019).
- [8] T.-N. Ye, Y.-F. Lu, J. Li, T. Nakao, H.-S. Yang, T. Tada, M. Kitano, and H. Hosono, *J. Am. Chem. Soc.* **139**, 17089 (2017).
- [9] Y. Toda, S. W. Kim, K. Hayashi, M. Hirano, T. Kamiya, H. Hosono, T. Haraguchi, and H. Yasuda, *Appl. Phys. Lett.* **87**, 254103 (2005).
- [10] Z. Yu, H.-Y. Geng, Y. Sun, and Y. Chen, *Sci. Rep.* **8**, 3868 (2018).
- [11] M. Miyakawa, S. W. Kim, M. Hirano, Y. Kohama, H. Kawaji, T. Atake, H. Ikegami, K. Kono, and H. Hosono, *J. Am. Chem. Soc.* **129**, 7270 (2007).
- [12] H. Tamatsukuri, Y. Murakami, Y. Kuramoto, H. Sagayama, M. Matsuura, Y. Kawakita, S. Matsuishi, Y. Washio, T. Inoshita, N. Hamada, and H. Hosono, *Phys. Rev. B* **102**, 224406 (2020).
- [13] J.-H. Hou, K.-X. Tu, and Z.-F. Chen, *J. Phys. Chem. C* **120**, 18473 (2016).
- [14] J.-P. Hu, B. Xu, and S.-Y. Yang, *ACS Appl. Mater. Interfaces* **7**, 24016 (2015).
- [15] S. Y. Lee, J.-Y. Hwang, J. Park, C. N. Nandadasa, Y. Kim, J. Bang, K. Lee, K. H. Lee, Y.-W. Zhang, Y.-M. Ma, H. Hosono, Y. H. Lee, S.-G. Kim, and S. W. Kim, *Nat. Commun.* **11**, 1526 (2020).
- [16] Y. Mudryk, D. Paudyal, V. K. Pecharsky, and K. A. Gschneidner, *J. Appl. Phys.* **109**, 07A924 (2011).
- [17] S.-Y. Liu, C.-Z. Wang, L.-L. Liu, J.-H. Choi, H.-J. Kim, Y. Jia, C. H. Park, and J.-H. Cho, *Phys. Rev. Lett.* **125**, 187203 (2020).
- [18] J. Chae, J. Lee, Y. Oh, and G. Kim, *Phys. Rev. B* **104**, 125403 (2021).

- [19] J. Zhou, Q. Wang, Q. Sun, X. S. Chen, Y. Kawazoe, and P. Jena, *Nano Lett.* **9**, 3867 (2009).
- [20] H. Gonzalez-Herrero, J. M. Gamez-Rodriguez, P. Mallet, M. Moaied, J. J. Palacios, C. Salgado, M. M. Ugeda, J.-Y. Veuillen, F. Yndurain, and I. Brihuega, *Science* **352**, 437 (2016).
- [21] X.-L. Qiu, J.-F. Zhang, Z.-Y. Lu, and K. Liu, *J. Phys. Chem. C* **123**, 24698 (2019).
- [22] P. Hohenberg and W. Kohn, *Phys. Rev.* **136**, B864 (1964).
- [23] W. Kohn and L. J. Sham, *Phys. Rev.* **140**, A1133 (1965).
- [24] G. Kresse and J. Furthmüller, *Comput. Mater. Sci.* **6**, 15 (1996).
- [25] G. Kresse and J. Furthmüller, *Phys. Rev. B* **54**, 11169 (1996).
- [26] J. P. Perdew, K. Burke, and M. Ernzerhof, *Phys. Rev. Lett.* **77**, 3865 (1996).
- [27] S. L. Dudarev, G. A. Botton, S. Y. Savrasov, C. J. Humphreys, and A. P. Sutton, *Phys. Rev. B* **57**, 1505 (1998).
- [28] S. Baroni, S. de Gironcoli, A. Dal Corso, and P. Giannozzi, *Rev. Mod. Phys.* **73**, 515 (2001).
- [29] A. Togo, F. Oba, and I. Tanaka, *Phys. Rev. B* **78**, 134106 (2008).
- [30] X.-J. Wang, J. R. Yates, I. Souza, and D. Vanderbilt, *Phys. Rev. B* **74**, 195118 (2006).
- [31] A. A. Mostofi, J. R. Yates, G. Pizzi, Y.-S. Lee, I. Souza, D. Vanderbilt, and N. Marzari, *Comput. Phys. Commun.* **185**, 2309 (2014).
- [32] Q. Wu, S. Zhang, H.-F. Song, M. Troyer, and A. A. Soluyanov, *Comput. Phys. Commun.* **224**, 405 (2018).
- [33] See Supplemental Material at <http://link.aps.org/supplemental/10.1103/PhysRevB.106.045138> for band structures with SOC, molecular dynamics simulations at 300 K, and the energies, structures, magnetic configurations, and density of states of monolayer Gd<sub>2</sub>C with the partial and disordered H coverages.
- [34] S.-T. Zhao, Z.-Y. Li, and J.-L. Yang, *J. Am. Chem. Soc.* **136**, 13313 (2014).
- [35] D. L. Druffel, K. L. Kuntz, A. H. Woomer, F. M. Alcorn, J. Hu, C. L. Donley, and S. C. Warren, *J. Am. Chem. Soc.* **138**, 16089 (2016).
- [36] B. Huang, G. Clark, E. Navarro-Moratalla, D. R. Klein, R. Cheng, K. L. Seyler, D. Zhong, E. Schmidgall, M. A. McGuire, D. H. Cobden, W. Yao, D. Xiao, P. Jarillo-Herrero, and X. Xu, *Nature* **546**, 270 (2017).
- [37] X.-R. Li, Z.-N. Sun, J.-W. Li, H. Jin, J. Wang, and Y.-D. Wei, *J. Mater. Chem. C* **8**, 11369 (2020).
- [38] F.-Y. Li and Z.-F. Chen, *Nanoscale* **5**, 5321 (2013).
- [39] S.-L. Zhang, Y.-H. Hu, Z.-Y. Hu, B. Cai, and H.-B. Zeng, *Appl. Phys. Lett.* **107**, 022102 (2015).
- [40] Y. Cui, G. Zhang, H. Li, H. Lin, X. Zhu, H. Wen, G. Wang, J. Sun, M. Ma, Y. Li, D. Gong, T. Xie, Y. Gu, S. Li, H. Luo, P. Yu, and W. Yu, *Sci. Bull.* **63**, 11 (2018).
- [41] E. I. Rashba, *Phys. Rev. B* **62**, R16267 (2000).